Structural analysis of Fe/Ni(001) films by photoelectron diffraction

G. C. Gazzadi*

INFM-LDS, SS 14 km 163.5, 34012 Basovizza, Trieste, Italy

P. Luches, A. di Bona, L. Marassi, L. Pasquali, S. Valeri, and S. Nannarone

INFM and Dipartimento di Fisica, Università di Modena e Reggio Emilia, Via G. Campi 213/a, 41100 Modena, Italy

The structure of Fe films, epitaxially grown on Ni(001), has been studied in the 0–14 ML coverage range by means of photoelectron diffraction (PD) in the forward scattering regime. Quantitative analysis by a multiple scattering approach has been performed on Fe films at a coverage of 3 and 7 ML. Analysis of the 3-ML data showed that growth was not layer-by-layer but rather occurred through islands nucleation and that transition from the pseudomorphic fcc to the bcc phase was located in this early stage of growth. In fact, best fit was obtained by calculations on a 2 ML bcc$\langle 110 \rangle$/3 ML fcc(001) Fe film with the bcc$\langle 111 \rangle \| fcc\langle 110 \rangle$ in-plane orientation. Interlayer spacings of 2.05 ± 0.06 Å, 2.01 ± 0.03 Å, and 1.85 ± 0.03 Å were found in the bcc region, between bcc and fcc layers and in the fcc region, respectively. Best-fit in-plane nearest-neighbors (n-n) distance was 2.49 ± 0.02 Å, in registry with that of the Ni substrate. To analyze the 7-ML data a 4 ML bcc(110)/3 ML fcc(001) film was employed, varying the fitting parameters in the bcc region only. Best fit was obtained for an interlayer spacing of 2.04 ± 0.04 Å and in plane n-n distance of 2.47 ± 0.01 Å. At 14 ML the PD pattern collected over a 94° azimuthal range displayed symmetry around the [110] substrate direction, which was explained by the equipopulation of the 4 bcc(110) domains satisfying the bcc$\langle 111 \rangle \| fcc\langle 110 \rangle$ alignment.

I. INTRODUCTION

The face centered cubic (fcc) phase of Fe (γ-Fe) at low temperature has been the subject of many theoretical and experimental investigations due to the strong dependence of its magnetic properties on the atomic volume: the so-called magneto-volume instability.[1–5] As γ-Fe is stable in bulk phase only above 910 °C, epitaxial growth of thin-Fe films on suitable fcc substrates is needed to stabilize it at room temperature (RT). In this way, by forcing a pseudomorphic growth and playing with the value of the substrate lattice constant it is possible to tailor the Fe atomic volume in the growing film. Within this framework the detailed knowledge and control of the atomic structure and film growth plays a crucial role. The lattice constant of γ-Fe at RT, extrapolated from the high temperature phase, is equal to 3.59 Å.[6] Cu has been the most widely employed substrate, due to the good lattice match ($a_{Cu} = 3.61$ Å) and to the non-magnetic nature, which allows to single out the magnetic properties of the Fe overlayer.[4,5] The use of magnetic fcc templates, on the other hand, might add interest to the study of γ-Fe because novel magnetic phases could be stabilised under the influence of both structure and magnetism of the substrate. With this respect, Ni is suitable, its lattice constant being 3.52 Å (-2% lattice mismatch), and both theoretical and experimental studies have confirmed the influence of the substrate magnetism on the Fe overlayer.[7,8]

In this work we present a structural analysis of Fe films grown on Ni(001) performed by photoelectron diffraction (PD). Early studies of Fe growth on Ni(001) were performed by transmission electron microscopy[9,10] on hundreds Å-thick films grown in high vacuum. A strained fcc phase was found to form up to 8–9 ML, followed by transition to a bcc (110)

phase. More recently, low energy electron diffraction (LEED) was employed to study the growth in ultra high vacuum. Qualitative analysis by Lee, Abu-Jeudeh, and Montano[11] found evidence of fcc phase up to 6 ML, where possible formation of bcc (110) crystallites took place. A quantitative structural analysis by Lu *et al.*[12] interpreted LEED patterns up to 6 ML as originated by a strained fcc phase, with 8% interlayer distance expansion. At 10 ML the interlayer distance was found further expanded to 10%. A recent work by Schirmer and Wuttig[13] on a Ni(7 ML)/Cu(001) substrate observed an fcc phase up to a coverage of 11 ML and subsequent formation of a bcc(110) phase. Quantitative LEED analysis on the 6 ML-thick film gave bulk and first interlayer spacings 1% and 7% expanded relative to the Ni value, respectively. From the point of view of magnetism, O'Brien and Tonner[4] found, on Fe/Ni(001), a magnetic sequence similar to that of Fe/Cu(001) as a function of the Fe coverage and assigned the magnetic changes to crystalline phase transitions in the Fe film, calling for more detailed structural studies. Similar results were found by Kuch and Parkin[14] in studying Fe/Ni multilayers by x-ray Diffraction and Superconducting Quantum Interference Device. In a recent work,[15] we have analyzed Fe/Ni(001) films from the structural point of view, employing the primary-beam diffraction modulated electron emission (PDMEE) technique,[16] a powerful approach which provides quick qualitative analysis of thin films structure and it is easily feasible on most electron spectroscopy equipment. Fcc phase, tetragonally distorted along the growth direction, was observed up to 5 ML, followed by a transition to the bcc (110) phase which completed at 14 ML. In the first 3 ML evidence of Fe/Ni intermixing was found.

In the present work a quantitative approach is applied by

means of angle-scanned PD combined with multiple scattering (MS) calculations. The PD technique is a well established structural probe for surface and subsurface structural characterization.[17] In the forward scattering regime, i.e., for photoelectron energies $\geqslant 500$ eV, it enables detailed structural analysis by means of the shape and angular position of the forward focusing features, which are related to closed packed atomic chains. The aim of this work is twofold. First, to solve quantitatively the Fe film structure by fitting the data with multiple scattering calculations and, second, to support the validity of the PDMEE approach by comparing our previous results with the present ones. The paper is organized as follows. In Sec. II, the experimental details about sample preparation and measurements are given. In Sec. III, PD experimental results are shown. In Sec. IV, the best-fit MS calculations are reported divided into three subsections, corresponding to low, intermediate and high-coverage regions. Finally, in Sec. V, the discussion of results and conclusions are presented.

II. EXPERIMENT

Ni(001) surface was prepared by Ar^+ sputtering at 1.5 keV and annealing at 550 °C. Short O_2 exposures followed by flashes at 600 °C were used to eliminate the residual carbon segregated at the surface after annealing. Surface cleanness and local order were checked by photoelectron spectroscopy and PD measurements, respectively. Base pressure of the scattering chamber was 2×10^{-10} Torr, rising to 8×10^{-10} Torr during evaporations. Fe was evaporated by means of electron-bombardment cells, using 99,999% purity Fe rods. A deposition rate of 0.5 ML/min was calibrated by means of a quartz microbalance. PD measurements were performed at beamline 7.2 (ALOISA) (Ref. 18) at ELETTRA Synchrotron (Trieste, Italy). The beamline was operated in the undulator mode and a photon beam of energy $E = 850$ eV was focused into the scattering chamber by means of a grating-crystal monochromator system. Intensity angular distributions (IAD's) of Fe3p ($E_k = 797$ eV) and Ni3p ($E_k = 783$ eV) photoelectrons were collected by scanning the hemispherical analyser (1° angular resolution) over the polar take-off angle, in the plane containing the chosen azimuthal direction, laying on the sample surface, and the sample normal. Polar angles (θ) were measured with respect to the sample normal, azimuthal angles (ϕ) with respect to the [110] substrate direction. Polar scans were performed at angular steps of 1° and then fitted by a spline function at steps of 0.1°, in order to determine the forward features angular position with an uncertainty of ±0.1°. The PD pattern measured at a coverage of 14 ML was obtained by collecting IAD's over a 94° azimuthal range, centred around $\phi = 0$° at angular step $\Delta \phi = 2$°.

III. PD EXPERIMENTAL RESULTS

In Fig. 1 Ni3p and Fe3p IAD's along the [110] azimuth are shown for the clean Ni substrate and for Fe films over the 0–14 ML coverage range, respectively. Ni3p IAD is characterized by three major forward focusing features at 0°, 36.8°, and 55.9°, corresponding to the [001], [112], and [111] atomic chains, respectively. The relative intensity and shape
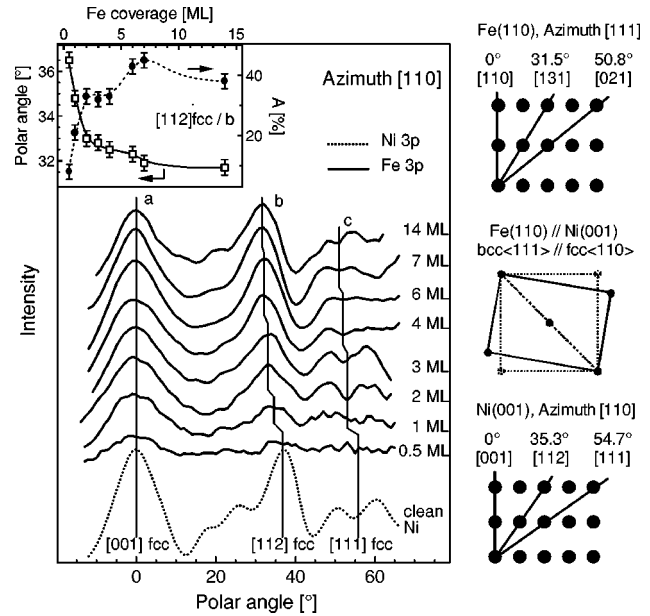

FIG. 1. Intensity angular distributions (IAD's) of the Ni 3p and Fe 3p photoelectrons for the clean Ni(001) surface and for Fe films at different coverage, respectively, along the [110] azimuth. In the inset, anisotropy (●) and angular position (□) of the [112]fcc/b feature are shown as a function of the Fe coverage. Cross sections of the Ni(001) and Fe(110) surfaces along the [110] and [111] azimuths, respectively, are sketched along with the relative orientation between Ni(001) and Fe(110) surface cells.

of these features are related to the inner structure of the corresponding atomic rows. [001] and [112] rows are closer packed than [111], thereby 0° and 36.8° features reflect a stronger focusing efficiency and are more intense and strongly peaked than the feature at 55.9°. The [111] feature is broad, with two symmetric peaks rounding a dip at the center, a so-called "volcano" shape typical of less densely packed atomic chains, generated by multiple scattering effects.[19] Fe IAD at 0.5 ML shows two weak features aligned with the [001] and [112] peaks of the Ni curve. At 1 ML they are better defined and the [112] feature is clearly shifted towards lower angles. Furthermore, a feature in the angular region corresponding to the [111] chain is rising. As the coverage increases the [112] peak angular position further shifts, from 33.0°, at 2 ML, to 31.7° at the final coverage of 14 ML, where the feature has been labeled as "b." In the inset of Fig. 1 the angular position and anisotropy [$A = (I_{max} - I_{min})/I_{mean}$] of the [112]fcc/$b$ peak are shown as a function of the Fe coverage. The behavior of the [111] feature is more peculiar. It undergoes an angular shift similar to that of [112], which brings its position from 53°, at 2 ML, to 51° at 14 ML, where the feature is labeled as "c." Moreover, a marked change is observed in its shape: between 2 and 3 ML the two peaks are well distinct and separated by a pronounced dip, then, at 4 and 6 ML, the doublet closes up almost in a single feature, and, from 7 ML on, the peaks reappear as distinct features.

The close resemblance between the Ni3p IAD and the Fe3p IAD's at low coverage suggests that the first Fe layers arrange pseudomorphically with the substrate, i.e., fcc(001). However, the angular position of the off-normal forward features, rapidly moving towards lower angles with the Fe cov-

erage, indicates that the Fe film is progressively strained along the normal direction by an expansion of the interlayer distance. In fact, assuming a lattice parameter of 3.59 Å for fcc Fe, the Fe surface cell must shrink by 2% to match with the Ni substrate and a vertical expansion is expected to compensate for the in-plane contraction. This expansion can be predicted on the basis of elastic strain calculations.[20] If the in-plane lattice constant of the substrate is adopted, a vertical expansion by 5%, relative to Ni value, results, corresponding to an interlayer spacing of 1.84 Å and a shift of the [112] feature by $-1.3°$. The angular position of the [112] feature rapidly drops with Fe coverage and keeps within the values expected from elastic strain theory only up to 1 ML. Above this coverage it further reduces, reaching 31.7° at the final coverage, a value which largely exceeds that predicted by theory. This behavior can be explained if a transition to the bcc(110) phase develops above 2-3 ML. In fact, by assuming a bcc$\langle 111 \rangle \| fcc\langle 110 \rangle$ in-plane orientation between the bcc(110) and fcc(001) surface cells, the lattice mismatch is only 0.1% and, along the bcc[111] azimuth, there are two closed-packed off-normal chains: the [131] at 31.5° and the [021] at 50.8°. These angular positions are very close to those assumed by the ''b'' and ''c'' features, respectively, in the 14 ML Fe IAD. The equilibrium interlayer distance between bcc(110) layers is 2.03 Å, in agreement with the increasing expansion deduced from the [112] peak shift. The behavior of the [112]fcc/*b* peak anisotropy (inset of Fig. 1) can also be interpreted within this model. On one hand it shows the usual trend expected for an epitaxial film of increasing thickness,[21] with a rapid increase at low coverage followed by a smooth stabilization to an equilibrium value at high coverage, where the film is bulklike. On the other hand, the marked step between 2 and 4 ML occurs exactly in the coverage region where the fcc-to-bcc transition locates on the basis of angular position data, and presumably reflects the structural changes occurring on topmost layers of the film.

On the basis of low coverage Fe IAD's, some considerations on the growth mode can be made. IAD's at 0.5 and 1 ML rule out layer-by-layer growth, because it would imply the absence of forward focusing features in this coverage region. This opens the possibility of either islands nucleation or intermixing between Fe and Ni atoms at the interface. In our previous study on the same system we concluded for intermixing.[15] In that case, best fit of Fe-to-Ni Auger intensity ratio occurred assuming an Fe/Ni intermixing extended over 3 layers and the [112] peak position in the Fe IAD's kept aligned with that of the Ni substrate up to 3 ML, as expected for Fe atoms embedded in a Ni matrix. In the present case, on the contrary, we notice that: (i) the [112] feature is shifted by $-1.4°$ already at 1 ML and (ii) the Ni3*p* IAD's collected at low-Fe coverage (not shown here) do not show any appreciable angular shift of the main off-normal features. Therefore, the formation of islands thicker than the nominal coverage, rather than intermixing, is strongly suggested. The different conclusion drawn in our previous experiment can be explained by the great influence that small variations in growth conditions and sample preparation can have in determining the growth mode and structure of the film, particularly in the early stages.

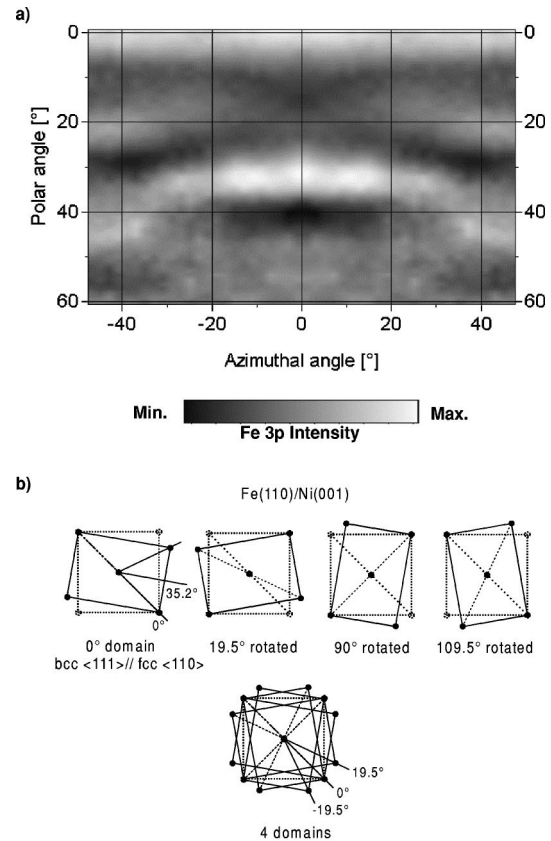At a coverage of 14 ML we measured Fe3*p* IAD's over a

FIG. 2. (a) Fe 3*p* IAD's collected over a wide azimuthal range on the 14-ML Fe film. (b) Sketch of the four possible bcc(110) domains orientation relative to the Ni(001) surface cell and of their superposition.

94° azimuthal range, centered around the [110] substrate azimuth. The experimental pattern, shown in Fig. 2(a), is characterized by the following features: (i) data display a symmetry around the [110] substrate direction, the 0° azimuth (after verifying the symmetry of raw data with respect to the [110] azimuth, Fig. 2(a) was obtained by averaging polar IAD's at equivalent azimuths), (ii) a high-intensity region between 30°–35° polar angles, corresponding to the bcc[131] forward feature, extends over a $-20°$–20° azimuthal range, and (ii) a low-intensity, ''X-shaped'' region extends over the whole azimuthal range between 5°–30° polar angles. The symmetry around the [110] direction can be explained according to the model sketched in Fig. 2(b). There are four possible orientations between bcc(110) and fcc(001) cells satisfying the bcc$\langle 111 \rangle \| fcc\langle 110 \rangle$ relation. Aligning the bcc[111] direction with the fcc[110] one, we obtain the 0° domain. The three others arise by rotating this domain by 19.5°, 90° and 109.5°, in order to have all the possible alignments between the substrate and overlayer surface cell diagonals. None of the four bcc domains displays a symmetry around the [110] substrate direction, if considered alone. However, by a superposition of the four domains symmetry around 0° azimuth occurs, recovering the one observed in the experimental pattern. Therefore, the expected overall symmetry is fourfold instead of twofold, as for a single bcc(110) domain. The domains superposition also accounts for the extension of the bcc[131] forward feature over the $\pm 20°$ azimuthal range. It originates from the bcc{112}

atomic planes, containing the [131] atomic row, $\pm 19.5°$ apart from the 0° azimuth. The high-intensity feature in the experimental pattern, therefore, is a triplet composed by [131] peaks at $-19.5°$, 0°, and 19.5° azimuths.

IV. QUANTITATIVE ANALYSIS

The quantitative structural analysis was carried out by means of the MSCD code developed by Y. Chen and M. A. Van Hove,[22] performing MS calculations in the Rehr-Albers approximation. In our case, MS events up to the 5th order were considered. Phase shifts were calculated by the program up to angular momentum number $l = 25$, based on muffin-tin potentials taken from Ref. 23. The atomic cluster was defined by the radius r and the depth h of a semiellipsoid having the circular basis on the top layer and the vertex on the bottom one. In our calculations r was kept constant at 10 Å and h was varied according to the number of the layers involved.

As a first step, we searched for the best trial structure to be used in the fitting procedure by comparing the experimental data with calculations from films of different thickness and structural arrangement. In this comparison, the best qualitative agreement on the shape and relative intensity of the main features was considered, disregarding the exact match of forward features angular position. The latter, in fact, deals with a quantitative dependence on the structural parameters, and was determined by the true fitting procedure. Once the trial structure had been chosen, the best-fit procedure consisted in minimizing the R-factor upon variation of the fitting parameters. The R factor is defined as:

$$R = \Sigma_\theta [c\chi_c(\theta) - \chi_e(\theta)]^2 / \Sigma_\theta \{[c\chi_c(\theta)]^2 + \chi_e(\theta)^2\}, \quad (1)$$

where the calculated $[\chi_c(\theta)]$ and experimental $[\chi_e(\theta)]$ chi functions are given by

$$\chi_{c(e)}(\theta) = [I^{c(e)}(\theta) - I_0^{c(e)}(\theta)] / I_0^{c(e)}(\theta), \quad (2)$$

and $I^{c(e)}(\theta)$ is the calculated (experimental) photoelectron intensity as a function of the polar angle θ, $I_0^c(\theta)$ is the photoelectron intensity calculated without scattering effects and $I_0^e(\theta)$ is the response function of the detection system obtained by a spline fitting of $I^e(\theta)$; c is a constant normalizing $\chi_c(\theta)$ area to that of $\chi_e(\theta)$. The code allows automated fitting over different parameters, related to both structural and physical properties of the system, namely: in plane nearest-neighbors distance (a), interlayer spacing (d), Debye temperature (T_D), and inner potential (V_0). We focused our search on the structural parameters d and a, minimizing the R factor over a grid of values whose density was progressively increased approaching the R-factor absolute minimum. The error bar associated to a fitting parameter (p) was calculated according to the formula:[24] $\Delta p = (\varepsilon R_0 / N)^{1/2}$, where R_0 is the minimum value, $1/\varepsilon$ is the curvature of the R-factor curve calculated at the minimum and N is the number of independent data points over which the fit is performed. In our case, $N = 3$ was taken, corresponding to the number of major forward features along the [110] azimuth, which were supposed to be fairly independent of each other. Preliminarily, we tested the built-in fitting procedure of the code on the clean Ni(001) surface. In Fig. 3, the experimental Ni3p IAD
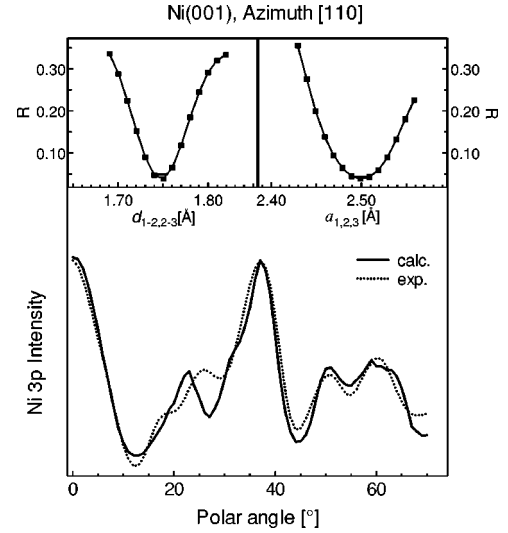

FIG. 3. Experimental and best-fit Ni3p IAD along the [110] azimuth for the clean Ni(001) surface. In the insets the R-factor behavior vs fitting parameters is shown; the segment sketches the fitting parameter error bar.

collected along the [110] azimuth is shown along with best-fit calculation on a eight-layer Ni(001) film. In the insets the R-factor curves are displayed as a function of the structural fitting parameters. The agreement between experimental and calculated curves is very good, for what concerns the main forward focusing features. In the 20°–30° angular region, on the contrary, where features generated by higher order interference and true diffraction occur, the agreement is not as good. This is probably due to the maximum number of atoms accepted by the code, which limits the in-depth extension of the cluster to 14.5 Å, when keeping the r parameter fixed to 10 Å. If the escape depth of the outgoing electrons is of the order of, or exceeds the cluster depth (in our case the inelastic mean free path was ~13 Å), bulk-related features like the aforementioned ones might not be correctly reproduced. On the other hand, a number of eight layers seems enough to describe correctly the scattering effects occurring along the closed-packed atomic rows, which provide the prominent structural information. The fitting was run over the interlayer spacing and the n-n in plane distance of the three topmost layers, i.e., $d_{1-2,2-3}$ and $a_{1,2,3}$, respectively. The absolute minimum was found for $d_{1-2,2-3} = 1.75 \pm 0.01$ Å, and $a_{1,2,3} = 2.50 \pm 0.01$ Å, practically identical, within the errors, to the values for the bulk material. These results agree with previous LEED studies,[25] reporting no substantial reconstruction for the Ni(001) surface. Fitting was also performed over V_0 and T_D parameters, finding the minimum for $V_0 = 13 \pm 6$ eV and $T_D = 170 \pm 60$ K. The large error bar associated with both quantities indicates the poor sensitivity of the R factor to these parameters, nevertheless, the inner potential value agrees with those reported in the literature.[25] On the contrary, the Debye temperature is much lower than the values reported for both bulk and surface of Ni. In the following calculations on Fe films, we shall not perform fitting over these parameters, assuming the values found for the Ni(001) surface.

A. Low coverage

To choose the best trial structure for fitting the 3-ML data we performed qualitative comparison with calculations (not

shown here) run on pseudomorphic fcc(001) films, 3, 4, and 5-layer thick, and on films composed by stacking 1 or 2 bcc (110) layers on top of 3 fcc (001) layers. The following trend was observed. Concerning fcc films, 3 and 4-layer thick films showed a very similar pattern, well reproducing the [001] and [112] features but not the [111]: in experimental data this feature is made up by two peaks at 49° and 58°, while in both calculations only a single peak at 58° appeared. The calculation on the 5-layer film better reproduced the [111] feature, showing a weak feature rising at 52° but, in this case, the [001] intensity was rather overestimated. Concerning the bcc/fcc films, the 1-layer bcc/3-layer fcc structure yielded a result very similar to that of the 4-layer fcc case. Adding the second bcc layer, on the contrary, markedly improved the agreement with data. The [111] feature doublet, in particular, was well reproduced by two peaks at 50° and 58°, and the agreement with [001] and [112] features remained good as well. Calculations were also performed on films with the fcc-like Fe_3Ni structure, in order to simulate intermixed Fe-Ni films. The results were indeed very similar to those obtained from fcc films of the corresponding thickness. From this comparison it can be concluded that: (i) the experimental data bear structural fingerprints of a film thicker than the nominal coverage and (ii) the 2-layer bcc/3-layer fcc film, rather than the 5-layer fcc or Fe_3Ni ones, seems the best trial structure. As shown in the previous section, at high coverage there is evidence of multidomain nucleation of the bcc(110) phase, to be considered when performing calculations on bcc layers. Unfortunately, it is not possible to define a multidomain cluster, which would correspond to the real physical case and an approximation has to be adopted. Along the [110] substrate azimuth the fourfold domain degeneracy reduces to two, the 0° and 109.5° and the 19.5° and 90° orientations being equivalent. We can thus consider the 0° and 19.5° domains only, whose cross-section along the aforementioned azimuth is represented by the {112} and {222} planes, respectively. {112} planes have three major atomic chains, the [110] at 0°, [131] at 31.5°, and [021] at 50.8°, with 4.05, 4.75, and 6.41 Å atomic spacing, respectively. The {222} planes are less densely packed, containing the [110] chain at 0°, the [121], at 30° and the [011] at 60°, with 4.05, 7.02, and 4.05 Å atomic spacing, respectively. As the main structural information in experimental data comes from the off-normal forward features located around 30° and 50°, we expect a major contribution from those atomic planes having the closest packed chains in this angular region, i.e., the {112} planes. Therefore, calculations involving bcc layers were run with the 0° domain orientation of the bcc(110) surface. The resulting best-fit parameters were then employed for a calculation on the 19.5° domain orientation and, eventually, the calculations from the two domains were combined and compared again to the experimental data in order to obtain a tentative estimate of the domains ratio.

In Fig. 4, the experimental Fe3p IAD for 3 ML coverage is displayed along with the best-fit calculation from the 2 ML bcc/3 ML fcc film. In the insets the R-factor curves are displayed as a function of the fitting parameters. The calculated curve shows an excellent agreement with data over the whole angular range. Both angular position and relative intensity of the three main forward features are matched. The fitting pro-
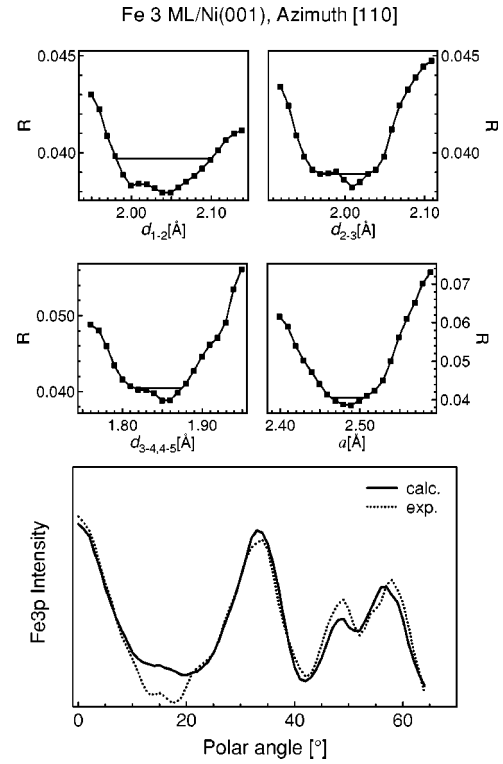

FIG. 4. Experimental and best-fit Fe3p IAD along the [110] azimuth for the 3-ML Fe film. Calculation is performed on a 2 ML bcc(110)/3 ML fcc(001) Fe layer. In the insets the dependence of the R factor vs fitting parameters is shown; the segment sketches the fitting parameter error bar.

cedure was run by varying four parameters independently: the interlayer spacing between bcc layers (d_{1-2}), bcc and fcc layers (d_{2-3}), and fcc layers ($d_{3-4}=d_{4-5}$) and the n-n in plane distance for the whole film (a). The absolute minimum was found to occur for the following values: $d_{1-2}=2.05 \pm 0.06$ Å, $d_{2-3}=2.01\pm0.03$ Å, $d_{3-4}=d_{4-5}=1.85\pm0.03$ Å, and $a=2.49\pm0.02$ Å. By a weighted combination of the 0° and 19.5° domain calculations a slightly lower R factor was obtained with 90% of 0° domain and 10% of 19.5° domain.

B. Intermediate coverage

To fit the experimental data at the intermediate coverage of 7 ML, it was assumed that the bcc phase extended from the fourth layer on, i.e., a 4 ML bcc/3 ML fcc structure was employed. In Fig. 5, the experimental Fe3p IAD and the best-fit calculation are shown. In the insets, the R-factor dependence on the fitting parameters is reported. The agreement between data and calculation is again very good. The fitting was performed by varying the structural parameters of the bcc layers only, namely: the interlayer spacing ($d_{1-2}=d_{2-3}=d_{3-4}$) and the n-n in plane distance ($a_{1,2,3,4}$). Variation over the structural parameters of the deeper fcc layers was found to be substantially ineffective on the R factor, therefore, the best-fit values obtained for the 3-ML data were maintained. The absolute minimum occurs for the following values: $d_{1-2,2-3,3-4}=2.04\pm0.04$ Å and $a_{1,2,3,4}=2.47\pm0.01$ Å. Further R-factor minimization over a weighted combination of the 0° and 19.5° domains yielded 70% of 0° domain and 30% of 19.5° domain.
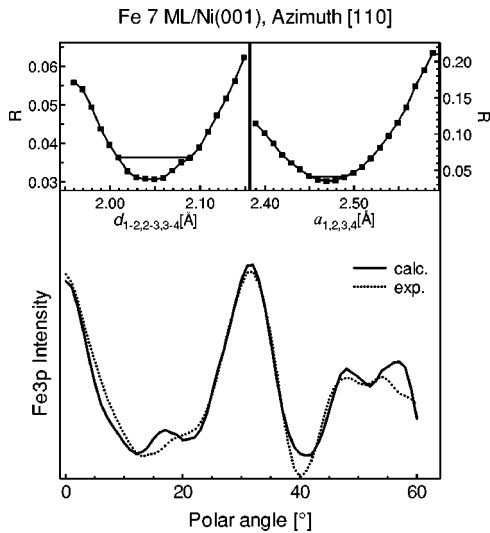
FIG. 5. Experimental and best-fit Fe3p IAD along the [110] azimuth for the 7-ML Fe film. Calculation is performed on a 4 ML bcc(110)/3 ML fcc(001) Fe layer. In the insets the dependence of the R factor vs fitting parameters is shown; the segment sketches the fitting parameter error bar.

C. High coverage

In Fig. 6, the experimental Fe 3p intensity pattern for the 14-ML film [Fig. 6(a)] is shown along with the calculation on a bcc(110) film with 0° domain orientation [Fig. 6(b)] and a superposition of calculations on the 4 domains, with equal weight for each [Fig. 6(c)]. All calculations are performed on a eight-layer thick bcc(110) film, with Fe(110) equilibrium lattice parameters. The calculation from the single domain clearly does not match the experimental pattern. In particular, the symmetry occurs around the 35° azimuth, as expected for a 0° domain [see Fig. 2(b)]. By a superposition of all the four possible domains, each weighted 0.25, the agreement between data and calculation remarkably improves, in particular, the symmetry around the 0° azimuth is recovered. The low-intensity X-shaped feature can be identified in the 5°–30° polar range, running over the whole azimuthal range and the [131] forward feature, between 30 and 35° polar angles, extends over the same azimuthal range observed for the experimental pattern.

V. DISCUSSION AND CONCLUSIONS

A summary of the quantitative analysis results for the clean Ni(001) surface and for the 3 ML Fe/Ni(001) and 7 ML Fe/Ni(001) films is listed in Table I. The structural evolution of the Fe film can be described as follows. Up to the 3rd/4th layer the Fe film grows pseudomorphically with the substrate, i.e., with a fcc(001) structure. However, the film is tetragonally strained along the growth direction, with an interlayer distance of 1.85 Å, 5% expanded over the Ni value. Above this critical thickness, the structural transition to the bcc(110) phase begins, with the bcc⟨111⟩‖fcc⟨110⟩ in-plane orientation. The spacing between the bcc and fcc layers is 2.01 Å and that between the first and second bcc layer is 2.05 Å, slightly expanded by 1% over the equilibrium Fe(110) value. The in-plane n-n distance on both bcc and fcc layers is found in registry with that of the substrate, i.e., 2.49 Å. As
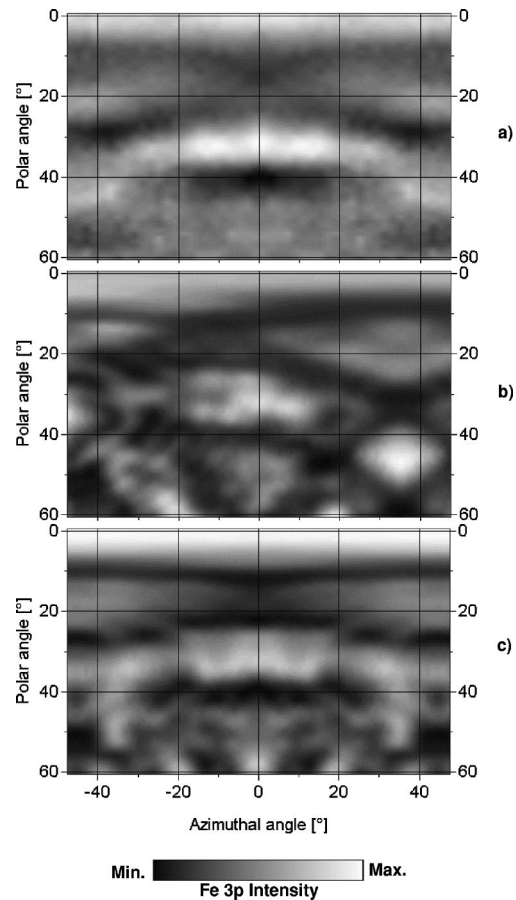

FIG. 6. (a) Experimental Fe 3p IAD's collected over a wide azimuthal range on the 14-ML Fe film. (b) Fe 3p intensity pattern calculated on a bcc(110) Fe film with 0° domain orientation. (c) Fe 3p intensity pattern obtained by a linear superposition of the calculations on bcc(110) Fe films with the 0°, 19.5°, 90°, and 109.5° domain orientations, equally weighted.

the number of bcc layers grows their interlayer distance relaxes to 2.04 Å, very close to the equilibrium value (2.03 Å), and the in plane n-n distance slightly reduces to 2.47 Å. At high coverage (14 ML), the Fe PD pattern collected over a wide azimuthal range displays a symmetry around the fcc[110] azimuth, which can be explained by an equal population of the four bcc(110) domains satisfying the bcc⟨111⟩‖fcc⟨110⟩ relation. Comparison of the fcc layer parameters with strain analysis calculations is very satisfactory: both the interlayer spacing and the in plane n-n distance agree with the predicted values. The parameters obtained for the bcc layers are very close to the equilibrium ones, as expected on the basis of the very small mismatch between pseudomorphic fcc(001) and bcc(110) unit cells along bcc⟨111⟩ and fcc⟨110⟩ directions. Compared to previous works performing quantitative structural analysis, our results are in good agreement with those of Lu et al.[12] who reported fcc (1×1) LEED patterns up to 6 Fe layers on Ni(001) and, above this coverage, the appearance of satellite spots attributed to bcc (110) islands. On a 2-ML film they found 1.90 Å and 1.85 Å Fe-Fe and Fe-Ni interlayer distances, respectively and, at 10 ML, still analysing the LEED pattern as fcc, they found interlayer spacing d_{1-2} and d_{bulk} of 2.04 Å and 1.94 Å, respectively. These results agree, within experimental errors, with ours for what concerns the interlayer distance

TABLE I. Best-fit parameters for the clean Ni(001) surface and for the 3- and 7-ML Fe films.

Experimental structural	Ni(001)	3 ML Fe/Ni(001)	7 ML Fe/Ni(001)
Best-fit structure	8 ML fcc ($R = 0.050$)	2 ML bcc/3 ML fcc ($R = 0.038$)	4 ML bcc/3 ML fcc ($R = 0.030$)
Best-fit Parameters (Å)	$d_{1-2,2-3} = 1.75 \pm 0.01$ $a_{1,2,3} = 2.50 \pm 0.01$	$d_{1-2} = 2.05 \pm 0.06$ $d_{2-3} = 2.01 \pm 0.03$ $d_{3-4,4-5} = 1.85 \pm 0.03$ $a = 2.49 \pm 0.02$	$d_{1-2,2-3,3-4} = 2.04 \pm 0.04$ $d_{4-5} = 2.01 \pm 0.03$ $d_{5-6,6-7} = 1.85 \pm 0.03$ $a_{1,2,3,4} = 2.47 \pm 0.02$

between fcc layers at low coverage. Those for the 10-ML film are difficult to compare, being possibly affected by the LEED analysis in terms of an fcc pattern despite the evidence of bcc(110) domains nucleation. The interlayer distance between the first and second layer, in fact, is the one expected for bcc(110) structure. Quantitative LEED analysis by Schirmer *et al.* was performed on 6 ML Fe/8 ML Ni(001)/Cu(001) trilayer. The pattern was analyzed as fcc(001) and the best-fit parameters were: $d_{1-2} = 1.88$ Å, $d_{bulk} = 1.78$ Å, and $a = 2.54$ Å. The main discrepancy with our results regards the in-plane *n-n* spacing, which is not in registry with that of the substrate but sensibly larger. This explains the reduced interlayer distance expansion found in the bulk of the film. The d_{1-2} value, however, is close to the interlayer distance we found in the fcc region.

Concerning the growth mode, both qualitative and quantitative analysis of Fe data at low coverage suggest that island nucleation occurs at this early stage. In particular, the fact that best fit of the 3-ML data is obtained with a 2 ML bcc/3 ML fcc structure indicates that the ''structural character'' at this coverage is mainly determined by regions thicker than the nominal value. Such a result can be explained as follows. At low coverage, when few scatterers compose the atomic chains, a stronger forward focusing effect occurs the longer the chain. Therefore, if the layer thickness is not homogeneous, we expect that thicker regions give a major contribution to the PD pattern compared to the thinner ones. Best fit of the 7-ML data is obtained with the nominal number of Fe layers, suggesting that island might coalesce forming a layer of uniform thickness as the coverage increases, in agreement with literature results.[13]

From the point of view of the magnetism of the Fe γ-phase, the atomic volume in the fcc region, as obtained from the best-fit parameters, is 11.5 Å^3. This value, on the basis of both spin dependent calculations[3] and experimental findings on Cu(001),[5] should be too small to induce ferromagnetic (FM) coupling. However, the possibility of polarization effects induced by the Ni substrate cannot be excluded. In the bcc region the calculated atomic volume is the equilibrium one (11.8 Å^3), and the coupling, of course, is expected to be FM.

Finally, comparison with results of our previous study is satisfactorily on the whole, and confirms the reliability of the PDMEE technique for quick on campus structural investigations. There, we concluded that, within the first 5 ML, the Fe film was fcc(001) strained by a 4% expansion along the normal direction and intermixing with the substrate, extended over the first 3 ML, occurred. At higher coverages a transition to the bcc(110) phase was suggested, having the bcc$\langle 111 \rangle \| fcc\langle 110 \rangle$ in-plane orientation and displaying multidomain character. The present results, as far as the structural evolution is concerned, closely recover those conclusions. In particular, both the quantitative estimate of the fcc phase strain, and the transition to the bcc(110) phase are reproduced. A discrepancy remains in describing the growth mode, which, as already mentioned, can be strongly sensitive to small variations in substrate preparation and growth conditions.

*Author to whom correspondence should be addressed. Mailing address: INFM e Dipartimento di Fisica, Università di Modena e Reggio Emilia, via Campi 213/a, 41100 Modena, Italy. Electronic address: gazzadi@unimo.it

[1] C. S. Wang, B. M. Klein, and H. Krakauer, Phys. Rev. Lett. **54**, 1852 (1985).

[2] G. L. Krasko, Phys. Rev. B **36**, 8565 (1987).

[3] V. L. Moruzzi, P. M. Marcus, and J. Kübler, Phys. Rev. B **39**, 6957 (1989).

[4] W. L. O'Brien and B. P. Tonner, Phys. Rev. B **52**, 15 332 (1995), and references therein.

[5] M. Wuttig, B. Feldmann, and T. Flores, Surf. Sci. **331–333**, 659 (1995).

[6] S. H. Lu, J. Quinn, D. Tian, and F. Jona, Surf. Sci. **209**, 364 (1989).

[7] R. Wu and A. J. Freeman, Phys. Rev. B **45**, 7205 (1992).

[8] G. B. Fratucello, A. M. Prandini, P. Luches, A. J. Patchett, S. D'Addato, and S. Nannarone (unpublished).

[9] D. C. Hothersall, Philos. Mag. **15**, 1023 (1967).

[10] J. W. Matthews and W. A. Jesser, Philos. Mag. **20**, 999 (1969).

[11] Y. C. Lee, M. Abu-Joudeh, and P. A. Montano, Surf. Sci. **143**, 469 (1984).

[12] S. H. Lu, Z. Q. Wang, D. Tian, Y. S. Li, F. Jona, and P. Marcus, Surf. Sci. **221**, 35 (1989).

[13] B. Schirmer and M. Wuttig, Surf. Sci. **399**, 70 (1998).

[14] W. Kuch and S. S. P. Parkin, J. Magn. Magn. Mater. **184**, 127 (1998).

[15] P. Luches, G. C. Gazzadi, A. di Bona, L. Marassi, L. Pasquali, S. Valeri, and S. Nannarone, Surf. Sci. **419**, 207 (1999).

[16] S. Valeri and A. di Bona, Surf. Rev. Lett. **40**, 141 (1997).

[17] C. S. Fadley, in *Synchrotron Radiation Research: Advances in S/urface and Interface Science*, edited by R. Z. Bachrach (Plenum, New York, 1992); W. J. Egelhoff, Jr., in *Ultrathin Magnetic Structures*, edited by J. A. C. Bland and B. Heinrich (Springer-Verlag, Berlin, 1994).

[18] L. Floreano, G. Naletto, D. Cvetko, R. Gotter, M. Malvezzi, L. Marassi, A. Morgante, A. Santaniello, A. Verdini, F. Tommasini, and G. Tondello, Rev. Sci. Instrum. **70**, 3855 (1999).

[19] M. L. Xu and M. A. Van Hove, Surf. Sci. **207**, 215 (1989).

[20] Details of the calculations are reported in P. Luches, Ph.D. thesis, University of Modena, 1998; see also P. M. Marcus and F. Jona,

Surf. Rev. Lett. **1**, 15 (1994); J. Phys. Chem. Solids **53**, 1513 (1994).

[21] S. Valeri, A. di Bona, and F. Borgatti, Surf. Sci. **371**, 143 (1997).

[22] Y. Chen, F. J. G. de-Abajo, A. Chasse, R. X. Ynzunza, A. P. Kaduwela, M. A. Van-Hove, and C. S. Fadley, Phys. Rev. B **58**, 13 121 (1998).

[23] V. L. Moruzzi, J. F. Janak, and A. R. Williams, *Calculated Electronic Properties of Metals* (Pergamon, New York, 1978).

[24] H. B. Nielsen and D. L. Adams, J. Phys. C **15**, 615 (1982).

[25] J. E. Demuth, P. M. Marcus, and D. W. Jepsen, Phys. Rev. B **11**, 1460 (1975); R. Feder, S. F. Alvarado, E. Tamura, and E. Kisker, Surf. Sci. **127**, 83 (1983).